ORIGINAL PAPER

Efficiency improvement in linear-move sprinkler systems through moderate runoff–runon control

M. J. Rossi · J. O. Ares

Abstract Given the importance of achieving substantial water and operation savings, automated irrigation management has evolved toward integration of soil moisture measurements with simulation models. The main objective of this study was to develop a set of procedures to maximize irrigation efficiencies in linear-move irrigation systems. A system of field truth data collection and spatially distributed, physically based hydrological modeling was developed to evaluate the efficiencies of linear-move systems considering various naturally occurring boundary conditions and management options. Interactions among the irrigation flow depth, the evaporation conditions, the net infiltration depth and soil moisture uniformity, the irrigation turn duration and runoff–runon production were considered. Environments were of the semiarid Patagonian Monte at varying field slope and antecedent soil moisture. Plot experiments on infiltration and overland flow were used to calibrate a modified version of the CREST hydrological model adapted to the simulation of linear-move irrigation. Modeling results show that irrigation efficiencies can be improved by allowing runoff–runon to occur to an extent compatible with adequate soil moisture uniformity at the end of the irrigation turns. High efficiencies in both attaining effective infiltration depths and minimizing irrigation turn durations may be reached by adjusting the irrigation flow depth through the advance velocity of the irrigation system and/or inter-nozzle distances with due consideration to the antecedent soil moisture condition and the field slope.

Abbreviations

BCMF	Boundary conditions and management factors
CREST	Coupled routing and excess storage
DDM	Drainage (flow) direction map (8-cell convention)
DEM	Digital elevation map
EM	Evaporation flow map
FAM	Flow accumulation factor (number of contributing upstream map cells)
GPS	Global positioning system
IIM	Irrigation intensity map
RRM	Runoff–runon depth map
TDI	Tension disk infiltrometer

List of symbols

θ_i	Soil moisture depth at location i (mm)
$\theta_{l,\mathrm{irr}}$	Soil moisture depth increase due to irrigation (mm)
θ_v	Soil moisture content (mm^3/mm^3)
$\bar{\theta}_{l,a}$	Average antecedent soil moisture depth (mm)
$\bar{\theta}_v$	Average volumetric soil moisture depth (mm^3/mm^3)
$\bar{\theta}_{l,\mathrm{end}}$	Average soil moisture depth at the end of irrigation turn (mm)
$\bar{\theta}_{l,\mathrm{irr}}$	Average soil moisture depth increase due to irrigation (mm)
σ_{RRF}	Standard deviation of runoff–runon factor
$\sigma_{\theta v}$	Standard deviation of volumetric soil moisture depth (mm^3/mm^3)
a, b, c	Coefficients of infiltration function (mm/min)
A_i	Irrigated area (mm^2)
CU	Coefficient of uniformity (%)

M. J. Rossi (✉) · J. O. Ares
National Patagonic Centre, CONICET, Boulvd. Brown 2915,
9120 Puerto Madryn, Chubut, Argentina
e-mail: rossi@cenpat-conicet.gob.ar

DS	Depressional storage area (%)
e_a	Irrigation application efficiency (mm/mm)
e_t	Irrigation turn duration efficiency (mm/min)
E_v	Evaporation flow (mm/min)
$\bar{E}_v$	Average value of the EM (mm/min)
F	Cumulative frequencies of θ_v at various class values
$I_{n,p}$	Infiltration flow fed from runoff–runon flow and ponded water (mm/min)
$I_{n,s}$	Infiltration flow fed from sprinklers (mm/min)
$I_{r,a}$	Cumulative irrigation flow depth (mm)
Irr	Irrigation flow (mm/min)
ITD	Irrigation turn duration (min)
K_{sat}	Saturated hydraulic conductivity (mm/min)
ND	Inter-nozzle distance (m)
NIC	Number of irrigated cells in field digital map
NRR	Number of cells where runoff–runon occur
$pCoem$	Overland flow friction factor
$pLeaOne$	Coefficient of non-depressional storage (100-DS)/100 (%)
RR	Runoff–runon depth (mm)
RRF	Runoff–runon factor
$\overline{RR}$	Average value of the RRM (mm)
$\overline{RRF}$	Average runoff–runon factor (all scenarios)
S	Field main slope (%)
TWI	Topographic Wetness Index
V	Velocity of the linear-move irrigation system (m/min)

Introduction

Irrigation is an increasingly important practice for sustainable agriculture in the arid and semiarid regions of the world. The expansion of irrigated agriculture has greatly increased crop productivity, stability and diversification in semiarid areas (Causapé et al. 2004). Without appropriate management, irrigated agriculture can be detrimental to the environment and endanger sustainability (Fernández-Cirelli et al. 2009). In most countries, agricultural demand for water ranges from 40 to 80 % of total consumption (Bazzani 2005), and efforts to maximize the efficiency of irrigation will have to increase to irrigate the same land area with fewer resources. Automated irrigation systems have a number of advantages, as compared with manual systems, including greater precision and reduction in human error (Castanon 1992) which leads to an increase in crop yields and savings in water, energy and labor costs (Mulas 1986).

Sprinkler irrigation system can be easily automated (Morvant et al. 1997; Uva et al. 1998) and can achieve high application efficiencies (McLean et al. 2000). The flexibility of present-day sprinkler equipment and its efficient

control of water application make the method almost universally applicable. A common, worldwide used, irrigation method is the linear-move sprinkler system. Their operation is usually synchronized in various ways to soil moisture sensor nets in order to supply water in accordance with specified target levels. Considerable sophistication involving the regulation of advance velocity and irrigation flow according to soil and atmospheric physical conditions is required to improve water use efficiency in these systems (Gencoglan et al. 2005).

At the beginning of an irrigation turn, the irrigation flow is usually lower than the infiltration rate and all the water applied infiltrates into the soil (Gencoglan et al. 2005). With time, the infiltration rate decreases and becomes lower than the irrigation rate (Mao et al. 2008). When irrigation continues after this point, superficial water flow and runoff–runon (overland flow and infiltration thereof) occur (James 1988; James and Larson 1976; Mein and Larson 1973; Mao et al. 2008). The rate of overland flow on a sloping field depends on the amount of water that can accumulate on the rough soil surface or its depressions. Runoff–runon and surface depression storages imply additional areas of water infiltration that remain active for some time after the pass of the irrigation machine. Time is also relevant to irrigation efficiency. If irrigation is completed in a short time, operation and maintenance costs decrease (Gencoglan et al. 2005) and water would be saved due to the reduction in evaporation. Efficient irrigation planning involves achieving maximum infiltration rates in minimum operation times.

Ceballos et al. (2002) explain that in semiarid regions with prevailing sandy soils, water infiltration is fast, and overland flow is limited as a consequence of the macroporosity of the soils. However, complex interactions of runoff generation, transmission and reinfiltration over short temporal scales (Li et al. 2011; Reaney 2008) have been observed in such soils, which add difficulties in the estimation of infiltration and overland flows. In arid/semiarid areas, the soil surface can be predominantly flat and gently sloped at extended spatial scales, and the superficial water flow occurs in very shallow structures combining small overland flow areas interspersed with finely ramified fingering patterns of small channels. Composite patterns of overland flow (Parsons and Wainwright 2006; Smith et al. 2011) can be expected to produce spatially heterogeneous patterns of water infiltration in the upper soil (van Schaik 2009).

Superficial water flow or runoff–runon flow on a rough surface is characterized by discontinuous puddle-to-puddle filling, spilling–merging and splitting dynamics (Chu et al. 2013), which involve a series of hydrodynamic, connected and individual ponding (depression storage sensu Antoine et al. 2011a) areas under the influence of surface

micro-topography. During a rain or irrigation event, the surface depressions can be filled gradually, resulting in the formation or evolution of dynamically connected wet areas. Usual procedures to study runoff-infiltration processes involve the use of hydrological models based on hydrograph records at a field scale. Although a large body of literature has been devoted to the criteria used to inspect hydrograph records (Ewen 2011), less attention has been paid to the fact that many hydrological models that can accurately reproduce hydrograph records, produce severely biased estimates of overland flow velocities (Mügler et al. 2011; Legout et al. 2012) or Reynolds-Froude numbers (Tatard et al. 2008) that characterize the friction characteristics of overland water flow.

Several studies have been conducted to investigate the hydrological connectivity of topographic surfaces and characterize the dynamic behavior of overland flow generation (Darboux et al. 2001; Antoine 2010; Antoine et al. 2009, 2011b; Appels et al. 2011). Other studies were conducted to investigate the effect of topographic surfaces (and related hydrological connectivity) on the infiltration flow. Leonard et al. (1999), Weiler and Naef (2003) and Ohrstrom et al. (2002), indicate that high terrain slope conditions usually correspond to low infiltration capacities, and the excess of available water that begins to puddle or move on the soil surface participates in the runoff–runon flow (Hillel 1998; Liu et al. 2011).

Rodríguez and Martos (2010) developed a software tool for estimating field values of infiltration and roughness parameters of a surface irrigation event. Their inverse modeling technique identified Kostiakov's and Manning's parameters and the inflow stabilization time. Less effort has been conducted to investigate the effect of micro-topographic surfaces and the related hydrological connectivity on the spatial distribution of surface water and infiltration flows.

Several parameters are usually considered in evaluating the performance of an irrigation program. A relevant indicator to consider is the irrigation turn duration or time taken by the linear-move machine to pass through a field. At long irrigation turn durations (slow advance speed), more water can be infiltrated into the soil profile. This also means higher operational costs in terms of fuel used by the self-propelled irrigation machine, labor costs and electricity costs of the pumping equipment.

Irrigation uniformity is another central goal of the sprinkler irrigation system design (Keller and Bliesner 2000). There are many factors that affect the uniformity of sprinkler irrigation, including the sprinkler system, climatic conditions and field management practices (Zhang et al. 2013). The spatial distribution of irrigation may affect the water distribution in the root zone, with significant effects on crop yield (Warrick and Gardner 1983). Extensive research

has been made on the surface distribution of water from sprinklers (Christiansen 1941; Hart 1961; Elliot et al. 1980; Warrick 1983; Zhang et al. 2013). However, little work has been carried out to investigate the uniformity of the infiltrated depth of water in the soil profile at the end of the irrigation turn duration. Low values of coefficients of uniformity (CU) of infiltrated depth of water in the soil profile at the end of the irrigation turn duration often indicate an incorrect combination of the number, size and/or spacing of sprinklers (Tarjuelo et al. 1992).

The selection of an appropriate irrigation flow rate is also important in the irrigation scheduling to achieve high application efficiencies. Appropriate flows depend on boundary conditions such as antecedent soil moisture and field slope. Armindo et al. (2011) indicated that the efficiency of the irrigation systems can be increased by adjusting the amount of water applied to specific field conditions and developed a flow rate sprinkler to be used in center pivots or linear-moving irrigation systems, with potential for utilization in site-specific irrigation scheduling. The authors claimed that the development of appropriate flow rate sprinkler projects is becoming increasingly important for precision irrigation, because it allows the optimization of site-specific management and aims to either reduce the use of water for production or increase the current levels of production with the same levels of water consumption. DeBoer et al. (2000) claim that it is difficult to predict the impact of increased wetted areas on surface runoff since each field situation is unique and must be considered on its merit. They also claim that before irrigation industry professionals can assess and make recommendations regarding an appropriate sprinkler selection for a given crop and soil scenario, an acceptable procedure based on reliable data and field evaluations must be established.

The complexity of the interactions among effects dictated by the underlying physics of the movement of water in the soil, the engineering aspects of automated irrigation and the economies of the operation prompted the use of simulation models to seek adequate compromises of time, costs, uniformity and efficient water use (Li and Kawano 1996; Silva 2007; Armindo et al. 2011). The use of simulation models enables the reduction in water consumption and increases the efficiency in the use of this resource (Montero et al. 2001). Modeling approaches are required to support improved use of linear-move sprinkler irrigation systems including the consideration of different configurations of inter-nozzle spacing, discharge rates and system speed to select the most efficient one in terms of surface soil moisture distribution and runoff–runon production in semiarid regions where evaporation loses are important (Wilmes et al. 1993; Molle and Legat 2000).

Simulation models of irrigation systems prove to be useful for different systems. Connell et al. (1999) generated a

predictive model for water and salt movement within irrigation bays in Australia; their objective was to provide a framework to investigate questions of irrigation practice and bay design for different site characteristics and to determine the optimal management arrangements for flood irrigation. Jorge and Pereira (2003) developed AVASPER for sets of sprinkler systems. MIRRIG (Pedras and Pereira 2006) is aimed for use in micro-irrigation systems. Merot and Bergez (2010) developed a model (IRRIGATE), based on existing knowledge and adapted models and new modules based on experiments and survey data to help water managers and agricultural advisors to manage water for gravity irrigation of hay cropping systems.

The Coupled Routing and Excess STorage (CREST) model is a distributed hydrologic model developed at the University of Oklahoma (http://hydro.ou.edu) and NASA SERVIR Project Team to simulate the spatiotemporal variation of atmospheric, land surface and subsurface water fluxes and storages by field cell-to-cell simulation (Wang et al. 2011). The grid cell resolution is defined by the user. The CREST components are: rainfall (irrigation)–runoff generation, evapotranspiration (or evaporation), sub-grid cell routing, downstream routing and feedbacks between the routing and rainfall (irrigation)–runoff modules. In each cell, a variable infiltration curve is employed to separate precipitation into runoff and infiltration. The model has been previously calibrated at the spatial scale of a basin and includes a subroutine to perform automated calibration based on hydrogram data.

This work presents a system of field truth data collection and spatially explicit hydrological modeling based on a modified CREST version adequate to evaluate the performance of linear-move irrigation systems in terms of the resulting soil moisture depth and uniformity, the irrigation efficiency and runoff–runon production in various field slopes and soil antecedent moisture configurations in semiarid regions. The results show that adequate combinations of managing factors (flow rates and turn length) result in improved water use efficiency depending on the terrain characteristics (slope and antecedent soil moisture). Allowing moderate amounts of runoff–runon improves irrigation efficiency at acceptable levels of post-irrigation soil moisture uniformity.

Materials and methods

Site descriptions

The micro-plot experiments used to estimate the input parameters for the sprinkler irrigation system model were performed at bare soil conditions in the Wildlife refuge "La Esperanza" (42°12′17.66″S, 64°59′1.29″O). The

hypothetical application of the sprinkler irrigation system model was based on a Digital elevation map (DEM) of a near field at "El Desempeño", (42°30′46.81″S, 64°44′37.46″O). Both sites correspond to the biogeographic unit Patagonian Monte (Argentina) and share vegetation, climate and soil characteristics.

The Patagonian Monte is a temperate region with a Mediterranean-like rainfall regime (Abraham et al. 2009). The mean annual temperature is 13.4 °C, and the mean annual precipitation is 235.9 mm (1982–2001). Soils are a complex of Typic Petrocalcids–Typic Haplocalcids (Soil Survey Staff 1999) with a fractured calcium carbonate layer from 0.45 to 1 m below the soil surface (del Valle 1998). Upper soil texture types (USDA) are sandy or loamy sand (Rossi and Ares 2012b), and volumetric soil moisture at field capacity is c.a. 25 % (Bisigato and Bertiller 1999; Rostagno et al. 1991). The average monthly evaporation (1970–1990) varies from 30 mm in the month of June to about 195 mm in January (Trelew, Instituto Nacional de Tecnología Agropecuaria).

There is a remarkable convergence between the semiarid area where this study was performed and similar areas in the northern hemisphere (Chihuahuan–Sonoran deserts). These areas correspond to the same climate subtypes, similar dominant vegetation and combinations of biological forms (Morello 1984 as quoted by Abraham et al., loc. cit.). Also, similar conditions are extensively found in arid and semiarid climates worldwide (Mares et al. 1985).

Field plot experiments and calibration of CREST model

Micro-plot ($\cong 80 \times 80$ cm) field experiments ($n = 4$) were performed to calibrate the sprinkler irrigation system model at the micro-plot scale and to estimate the model input parameters.

A DEM with x–y resolution 8 mm and z resolution ≤ 2 mm of each plot was constructed through a stereo-photogrammetry procedure (Rossi and Ares 2012a). Irrigation was supplied during varying time intervals (11–19 min) at rates 13.5–26.5 mm/min with a single nozzle on a small area (2.5–12.2 cm^2) of the plot. These rates were aimed to create a range of as high as possible water inflows to the soil that would encompass most usual irrigation rates used in linear-move systems (DeBoer et al. 2000) while maintaining laminar, subcritical hortonian runoff flow (Rossi and Ares 2012b). The irrigation procedure generated two subregions within each plot. One of them corresponded to the area that directly received water from the sprinklers. The second subregion corresponds to the area that did not receive water directly from the sprinklers, but received the excess of water (runoff–runon) from the first subregion.

The runoff flow areas were video-recorded. Video scenes at selected time intervals (1–4 min) were ortho-rectified,

and the instantaneous and successive flow areas were measured with image processing software (Idrisi v. 14.02, Clark Labs, Worcester) and used to estimate the fraction of the flow area occupied by depression storage (DS). This latter was achieved by identifying the areas where the overland flow front advance at each time interval occurred in the direction of increasing slope (Rossi and Ares 2012b).

Antecedent and post-irrigation soil moisture were measured by means of a pin-probe (50 mm) TDR (Time-Domain Reflect meter, TRIME®-FM, Ettlingen) at equidistant (30–35 mm) grid points covering the whole overland flow area and neighbor dry points.

Infiltration tests to obtain soil moisture-dependent infiltration curves to be used as input to the CREST model were performed using a tension disk (diameter = 45 mm) infiltrometer (TDI, Decagon Devices, Pullman, WA). Infiltration surfaces in the neighborhood of each plot were prepared by adding a 3 mm layer of silica sand (0.1–0.5 mm grain diameter) on the soil surface to improve hydraulic contact between the soil and the infiltrometer disk. Exponential equations were fitted (TableCurve 2D v.5.01, Systat Software Inc., San Jose, California) to relate the infiltration flow to the accumulated soil moisture. The infiltration estimates of the saturated hydraulic conductivity (K_{sat}) obtained with the TDI and the Wooding's (1968) model were compared ($R^2 = 0.46$, $P \leq 0.01$) with K_{sat} pedotransfer estimates (Rosetta v. 1.2, US Salinity Laboratory, Riverside) (Schaap and Leij 1998) based on textural data from soil cores ($n = 43$) obtained at the micro-plots and surrounding bare soil areas. Textural data of the upper (0–100 mm) soil were obtained with Lamotte's 1067 texture kit (LaMotte Co., Chestertown) calibrated with replicate estimates obtained at two reference laboratories (National Patagonic Centre, National University of the South, Argentina) with the Robinson's protocol (Gee and Bauder 1986). The bulk density of the upper soil was estimated through the excavation method (ISO #11272 1998). The technique involves determining the volume of an excavated hole using a plastic film inside the hole. The volume of the cast is determined by water displacement.

The model source code was modified to allow infiltration (runon) to occur under the area occupied by the runoff plume. An additional subroutine (CREST-IRRIGATION) was created in order to generate adequate irrigation depth data (at variable times, intensities and positions) for input to the model in the form of text files. Interflow (lateral movement of water in the vadose zone, Wang et al. 2011) was disregarded due to the short simulated duration of the experiments and the coarse textural characteristics of the soil. The directional digital map (DDM) and the flow accumulation map (FAM) were built based on the DEM through an 8-cell algorithm (Jensen and Domingue 1988). Both grids were estimated with the modules FLOW

Table 1 Input data to the CREST model: parameters and grids

Type	Name	Units	Meaning
P	*pCoem*	–	Overland flow friction factor
P	*pLeaOne*	%	Coefficient of non-depression storage
P	*a, b, c*	–	Coefficients of infiltration function
G	$\bar{\theta}_{l,a}$	mm	Average antecedent soil moisture depth
G	DEM	–	Digital elevation map (x–y resolution 0.08 m, z < 2 mm)
G	DDM	–	Drainage (flow) direction map (8-cell convention)
G	FAM	–	Flow accumulation map
G	*Irr*	mm/min	Irrigation flow
G	*Ev*	mm/min	Evaporation flow

P parameter, *G* Grid

and RUNOFF of the software Idrisi v. 14.02 (Clark Labs, Worcester), respectively.

Moisture estimates obtained with the TDR probe before application of water to the plots were used as input antecedent soil moisture ($\theta_{v,t=0}$) to the CREST model. Post-irrigation TDR estimates were used to create upper soil moisture maps of the overland plumes of each plot experiment, based on a nearest neighbor interpolation algorithm (Richards 1986). CREST θ_v estimates were updated at each run-time step (10 s) by adding the corresponding infiltration flow. Finally, TDR and CREST θ_v plume output maps were compared at the end of the irrigation period and checked for the runoff–runon plume speeds measured at its main axis (mm/s), the azimuth of its main axis (degrees), the average ($\bar{\theta}_v$) and standard deviation ($\sigma_{\theta v}$) of the soil moisture content at the end of the simulation time, the cumulative frequency distribution of soil moisture depth over the plot area and the fraction of the total area occupied by DS.

Input data used to calibrate the CREST model consisted in various parameters and grid data (Table 1). The automated option to calibrate CREST supplied within its code was discarded. The model calibration was performed by analyzing the characteristics of surface flow (average speed, orientation and extent of the wet plume), the extent of the DS area and soil moisture horizontal ($\bar{\theta}_v$, $\sigma_{\theta v}$) and vertical profiles. *pCoem* (the friction coefficient of overland flow) was obtained through inverse modeling. All other input parameters were based on measured field data (Table 1).

Analysis of scenarios of linear-move sprinkler irrigation

An altimetry survey of a near field (300 × 239 m) at "El Desempeño" was conducted by means of a high precision geodetic GPS receiver (LT4000HS, CHC, Shangai). Elevation was surveyed at 3,388 points spaced at
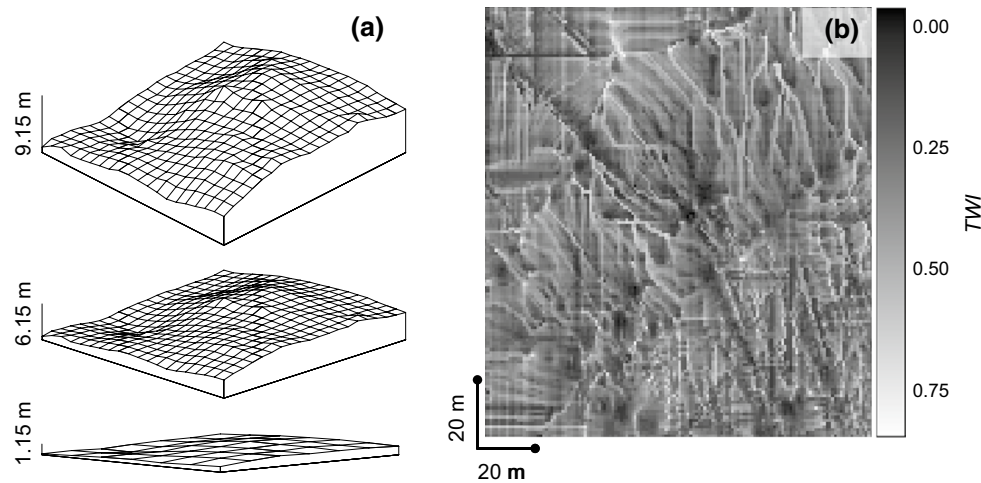
Fig. 1 Examples of CREST inputs. **a** DEMs (*x–y* resolution = 1 m) with different slope conditions (see Table 2) in the study area "El Desempeño" **b** Topographic Wetness Index (TWI) map used to generate antecedent soil moisture conditions

Table 2 Boundary conditions and management factors (BCMF) configurations used to model the irrigation scenarios

Condition	S (%)	V (m/min)	ND (m)	$\bar{\theta}_{l,a}$ (mm)
1	1.79	1.0	3.0	2.5
2	4.73	2.0	4.0	4.2
3	7.04	3.0	5.0	7.7

S: field main slope. $\bar{\theta}_{l,a}$: average antecedent soil moisture depth. V: velocity of the linear-move irrigation system. ND: inter-nozzle distance

* In following, scenarios are identified with acronyms referring to the various combinations of BCMF and their conditions. As an example, $S1V2ND3\bar{\theta}_{l,a}3$ correspond to low sloping terrain S, medium advance velocity V, high inter-sprinkler spacing ND, and high antecedent soil moisture $\bar{\theta}_{l,a}$

0.52 ± 0.005 m. These data were processed (semi-variogram and kriging interpolation) by geo-statistical modeling tools (Surfer v. 7, Golden Software Inc., Colorado) to construct a DEM of 1 m spatial resolution. A central subarea of the DEM (100 × 100 m) was selected to reduce computer load and was numerically processed to alter its original main slope (1.79 %) to obtain additional versions of the same with main slopes $S = 4.74$ % and $S = 7.74$ %, respectively (Fig. 1a). The DDM and FAM grids were estimated based on these as in the case of the plot experiments.

In order to specify the spatial distribution of antecedent soil water depth for use as input to the CREST model, a Topographic Wetness Index (TWI) was calculated using the SAGA (System for Automated Geoscientific Analyses; Olaya and Conrad 2009; Olaya 2004). This index indicates how prone a site is to become saturated, and its value is correlated with soil moisture. TWI is defined as the natural

logarithm of the ratio of a specific catchment area divided by the tangent of its main slope:

$$\text{TWI} = \ln\left(\frac{A}{\tan \alpha}\right) \tag{1}$$

where A (m²) is the contributing area or local upslope area draining through a certain point per unit contour length, and $\tan \alpha$ is the tangent of the local slope (Fig. 1b).

The TWI grid was rescaled to the range 0–1.00. The rescaled grid was alternatively multiplied by the values 5, 10 and 20, in order to simulate three hypothetical conditions of antecedent soil moisture depth ($\bar{\theta}_{l,a}$, mm) for input to CREST.

Scenarios ($n = 81$) of linear-move surface irrigation corresponding to irrigation turns at hypothetical preplanting/preemergence bare soil conditions were simulated through the CREST model. The scenarios were generated by combining possible boundary conditions (like soil slope and antecedent soil moisture) and management factors (like irrigation depth and turn duration) using the Latin hypercube sampling procedure (Ye 1998). The boundary conditions included three main slopes (S: 1.79, 4.73 and 7.04 %) and three average antecedent soil moisture depths ($\bar{\theta}_{l,a}$: 2.5, 4.2 and 7.7 mm). The management factors included three inter-nozzle distances (ND: 1.0, 2.0 and 3.0 m) and three velocities of the linear-move irrigation span (*V*: 1.0, 2.0 and 3.0 m/min) (Table 2). In what follows, scenarios will be identified through acronyms referring to the level (*1* = low; *2* = medium; *3* = high) of each combination of boundary conditions and management factors (BCMF) to ease their inter-comparison. As an example, $S2V1ND1\bar{\theta}_{l,a}3$ identifies a scenario where $S = 4.73$ %, $V = 1$ m/min, $ND = 3$ m $\bar{\theta}_{l,a} = 7.7$ mm, etc.

The irrigation system consisted in a 100 m span equipped with 20–33 sprinklers. The simulated sprinklers were of the SPINNER rotary type (Nelson Manufacturing Co. Inc., Washington, USA) at no-wind, 100 kPa water inflow pressure, 10 m water reach and 2.5 m elevation above ground, supplying an average irrigation depth of 8.2 mm/h at the wetted area (DeBoer et al. 2000). The spatial distribution of irrigation depth data around such sprinklers as estimated by these authors were fitted to a sixth degree polynomial equation:

$$y = 0.0003x^6 - 0.0066x^5 + 0.0576x^4 - 0.202x^3$$
$$+ 0.2383x^2 + 0.0032x + 0.9814; \quad R^2 = 0.8646; P < 0.001 \tag{2}$$

where y is an irrigation intensity factor (range 0–1), and x is the water range (m) of the sprinkler. This equation was used as input data in the CREST model in order to estimate the wetting pattern generated by the sprinklers at varying inter-nozzle distance (ND, m).

As in the plot experiments, an infiltration curve (infiltration variable with accumulated soil moisture depth) for use in CREST was fitted to data of 12 TDI experiments performed at "La Esperanza":

$$y = 0.041 + 0.084 \exp(-x/6.069); \quad R^2 = 0.36; P < 0.00001 \tag{3}$$

where y is the infiltration flow rate (mm/s), and x is the accumulated antecedent moisture (mm).

An uniform evaporation flow (4.3 mm/day) from the soil was simulated over the entire irrigated field. This is a typical daytime evaporation flow at spring time in the study area. DS was the average value of those at the plots used in the CREST model calibration.

The following output variables were obtained from CREST:

- Irrigation data: Number of irrigated cells (NIC), cumulative irrigation flow depth ($I_{r,a}$, mm), irrigation intensity (I_{rr}, mm/min) map (IIM), and irrigation turn duration (ITD, min) or time it takes the linear-move irrigation span to pass over the field plot.
- Soil data: the average soil moisture depth at the end of irrigation turn ($\bar{\theta}_{l,\text{end}}$, mm), the number of cells where runoff–runon occurred during the irrigation turn (NRR), the cumulative runoff–runon depth (mm) map (RRM) and the (isotropic and uniform in space) evaporation flow from the soil (E_v, mm/min) map (EM).

Since an important objective of irrigation is to incorporate to the soil profile a maximum of water depth in the shortest possible time, some terms specifically aimed to evaluate this performance aspect were defined. The average soil moisture depth increase due to irrigation ($\bar{\theta}_{l,\text{irr}}$, mm) or net infiltrated water depth was calculated as:

$$\bar{\theta}_{l,\text{irr}} = \bar{\theta}_{l,\text{end}} - \bar{\theta}_{l,a} \tag{4}$$

where $\bar{\theta}_{l,a}$ is the average antecedent soil moisture depth at the beginning of the simulation (mm).

An irrigation application efficiency (e_a) was calculated as the ratio of the net infiltrated water depth to the cumulative components of water consumption ($I_{r,a}$ and E_v):

$$e_a = \frac{\bar{\theta}_{l,\text{irr}}}{I_{r,a} + E_v} \tag{5}$$

where E_v is the cumulative water flow depth evaporated at the end of the irrigation turn (mm).

Also, an irrigation turn duration efficiency (e_t, mm/min) or ratio of net infiltrated water depth per unit of irrigation time was defined as:

$$e_t = \frac{\bar{\theta}_{l,\text{irr}}}{\text{ITD}} \tag{6}$$

A runoff–runon flow factor (RRF) was also calculated as:

$$\text{RRF} = \frac{\text{NRR}}{\text{NIC}} \tag{7}$$

A coefficient of uniformity (CU) of $\bar{\theta}_{l,\text{irr}}$ maps at the end of the irrigation turn was calculated as in Christiansen (1941):

$$\text{CU} = \left[1 - \frac{\sum_{i=1}^{m} \left| \theta_i - \bar{\theta}_{l,\text{end}} \right|}{m\bar{\theta}_{l,\text{end}}} \right] \times 100 \tag{8}$$

where θ_i is the soil moisture depth at location map cell i, and $\bar{\theta}_l = \left(\sum_{i=1}^{m} \theta_i \right)/m$ is the average soil moisture over all m map cells.

Stepwise regression models (SPSS, SPSS Inc., Chicago, IL) were performed in order to identify significant statistical associations among selected (normalized) CREST output variables.

Results and discussion

CREST: calibration with field plot experiments

The CREST model is a spatial explicit code that can be operated at user-defined spatial scales. The original version of the model was calibrated at 1 km grid size through the in-built automatic procedure supplied with the model code (Wang et al. 2011). In this work, the CREST model was calibrated at 1 m grid size through ground-truth data from micro-plots at a similar scale (0.8 m). The hydraulic properties of the runoff flows (laminar, subcritical) resulting from the experimental irrigation depths correspond to those expected from the operation of real sprinkler irrigation. Simulated runoff paths seldom exceeded 2–3 grid cells. These considerations

Table 3 CREST model calibration results through hydrological parameters obtained in field experiments

Plots	Parameters, units	Field data	CREST model
P01	Runoff–runon velocity, mm/s	0.42	0.34
	$\bar{\theta}_v$ at the end of irrigation, mm^3/mm^3	0.075	0.090
	σ_{θ_v} at the end of irrigation, mm^3/mm^3	0.039	0.048
	Main flow azimuth, degrees	335	349
	DS (% of the total area)	1.5	1.5
P02	Runoff–runon velocity, mm/s	0.21	0.22
	$\bar{\theta}_v$ at the end of irrigation, mm^3/mm^3	0.138	0.123
	σ_{θ_v} at the end of irrigation, mm^3/mm^3	0.105	0.065
	Main flow azimuth, degrees	188	173
	DS (% of the total area)	4.73	4.73
P03	Runoff–runon velocity, mm/s	0.23	0.22
	$\bar{\theta}_v$ at the end of irrigation, mm^3/mm^3	0.160	0.170
	σ_{θ_v} at the end of irrigation, mm^3/mm^3	0.083	0.099
	Main flow azimuth, °	203	215
	DS (% of the total area)	6.4	6.4
P04	Runoff–runon velocity, mm/s	0.21	0.18
	$\bar{\theta}_v$ at the end of irrigation, mm^3/mm^3	0.09	0.096
	σ_{θ_v} at the end of irrigation, mm^3/mm^3	0.066	0.099
	Main flow azimuth, degrees	229	211
	DS (% of the total area)	14.7	14.7

support the assumption that both spatial and hydraulic scale conditions were similar both in the field experiments used to calibrate the model and in its simulated scenarios.

The calibration of hydrology models is usually performed by comparison of the model behavior and measured hydrographs (Darboux et al. 2001; Antoine et al. 2009; Antoine 2010; Appels et al. 2011). However, it has been indicated (Darboux et al. 2002) that hydrographs not necessarily represent the spatio-temporal variations in the generation and evolution of surface flow processes on a surface. Many models that can accurately reproduce the hydrograph records produce biased estimates of surface flow rates (Mügler et al. 2011) or the flow friction parameters (Tatard et al. 2008). Additionally, not every system of hydrological interest can be instrumented with hydrograph support, and this is usually absent in irrigation situations.

In this study, the calibration of the CREST model at 1 m grid scale was based both on the surface flow properties and its relationship with the infiltration flow. Table 3 and Fig. 2 summarize the comparisons between field data and the model output. Figure 2 shows the soil moisture distribution at the four micro-plot experiments as at the end of the period of application of water and its comparison with the maps of distribution of soil moisture depth estimated with the CREST model.

Efficiencies in linear-move sprinkler irrigation systems under simulated scenarios of boundary conditions and management factors (BCMF).

Figure 3 shows an example of the spatial pattern of irrigation depth as generated by the subroutine CREST-IRRIGATION at variable run times (6, 23, 41 min) after the start of the irrigation turn. The example shown corresponds to an advance velocity of the linear-move system (*V*: 3.0 m/min) and SPINNER rotary sprinklers spaced at *ND*: 5.0 m.

Figure 4 presents examples of output maps obtainable from CREST by simulating two irrigation scenarios. Insets a–b are runoff–runon depth maps expected at mid-turn irrigation under two BCMF scenarios, and insets c–d show the corresponding soil moisture depth maps at the end of the irrigation turn. These output examples illustrate the effect of the slope, nozzle distance and antecedent soil moisture depth on the RR, $\bar{\theta}_{l,\mathrm{irr}}$ and e_a. The scenario $S1V3ND3\bar{\theta}_{l,a}1$ (a–c) is of lower $\bar{\theta}_{l,a}$, and higher *ND* than the scenario $S2V3ND1\bar{\theta}_{l,a}3$ (b–d), which results in lower RR, lower $\bar{\theta}_{l,\mathrm{irr}}$ and a more uniform distribution of soil moisture depth in c) than in d).

Low *ND*s (as in scenarios b–d of Fig. 4) imply high irrigation intensity and therefore high RR flows. Hillel (1998) and Liu et al. (2011) explain that when the irrigation intensity is greater than the soil infiltration rate, excess irrigation water begins to puddle or flow into the soil surface to form part of the surface flow. Under these conditions, runoff areas and/or DS areas are places where infiltration occurs even after the passage of the irrigation machine. The infiltration flow fed from runoff and DS areas is referred here as $I_{n,p}$, as different from $I_{n,s}$, the infiltration flow directly
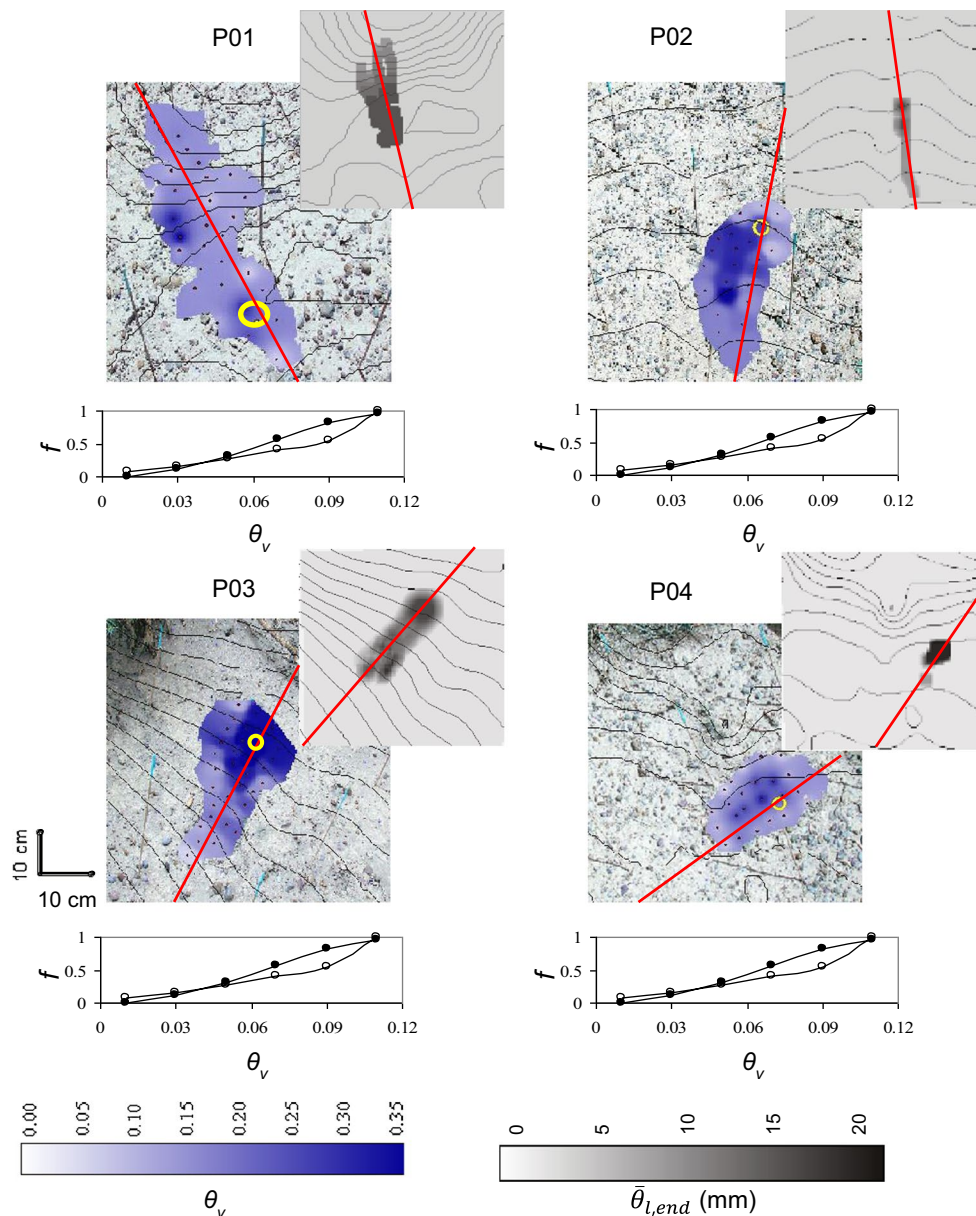
Fig. 2 Ortho-rectified photomaps of the experimental plots 01–04 (also see Table 3) used to calibrate CREST and spatial distribution of soil moisture content (θ_v) at the end of the irrigation interval, as measured with a TDR probe. *Contour lines* are at (01): 5 mm, (02): 10 mm, (03): 20 mm and (04): 5 mm spacing. *Yellow circles* indicate the irrigated areas. *Red lines* indicate the main azimuth flow direction measured from the center of water inflow areas. *Upper right insets* are the maps of soil moisture depth corresponding to the same plots obtained with the CREST model. Lower x–y graphs are the θ_v cumulative frequency (*f*) graphs corresponding to CREST (*white dots*) values and field data (*black dots*) (color figure online)

fed from sprinkler flow (Fig. 3). This implies that those scenarios with high irrigation intensities (low ND or low advance velocities *V*) generate more RR, which in turn results in an additional contribution to the total infiltration flow ($I_{n,s} + I_{n,p}$) and $\bar{\theta}_{l,\text{irr}}$.

Liu et al. (2011) observed in their simulated rain experiments that low rainfall intensities resulted in high infiltration rates and increased cumulative infiltration. Also, high infiltration rates are often observed at high rainfall or irrigation intensity, but it appears to be no consensus in the literature on the explanation of this behavior (Foley and Silburn 2002). The results of this study contribute to explain these apparent differences since water in the RR flow and in ponded areas (resulting from high irrigation intensity) contribute to the total infiltration flow.

An increment on the antecedent soil moisture depth $\bar{\theta}_{l,a}$ (Fig. 4) resulted in high RR flows. DeBoer et al. (2000) claim that it is difficult to predict the impact of the increase
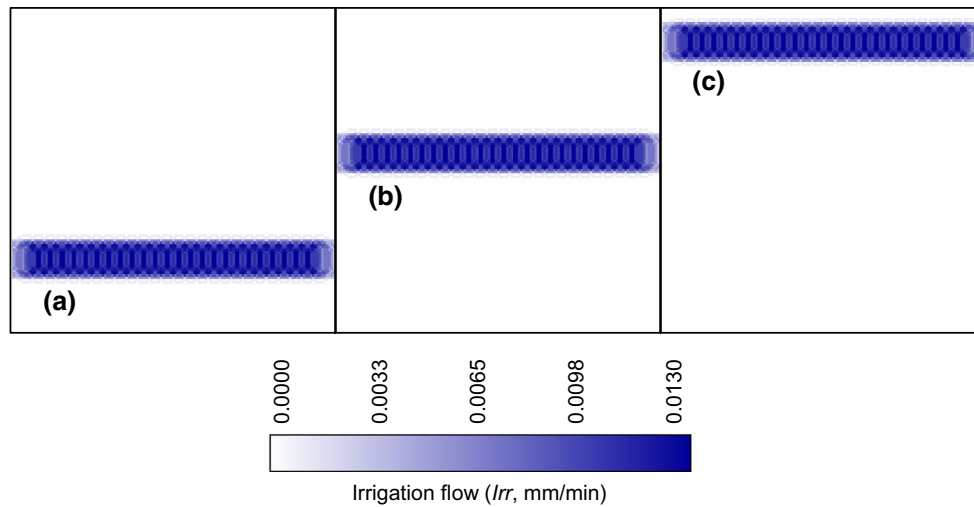
Fig. 3 Maps of the intensity of irrigation generated by the subroutine CREST-IRRIGATION. Scenarios are $S1V3ND3\bar{\theta}_{l,a}3$ (see also Table 2) at **a** 6 min, **b** 23 min, **c** 41 min after the start of the irrigation turn
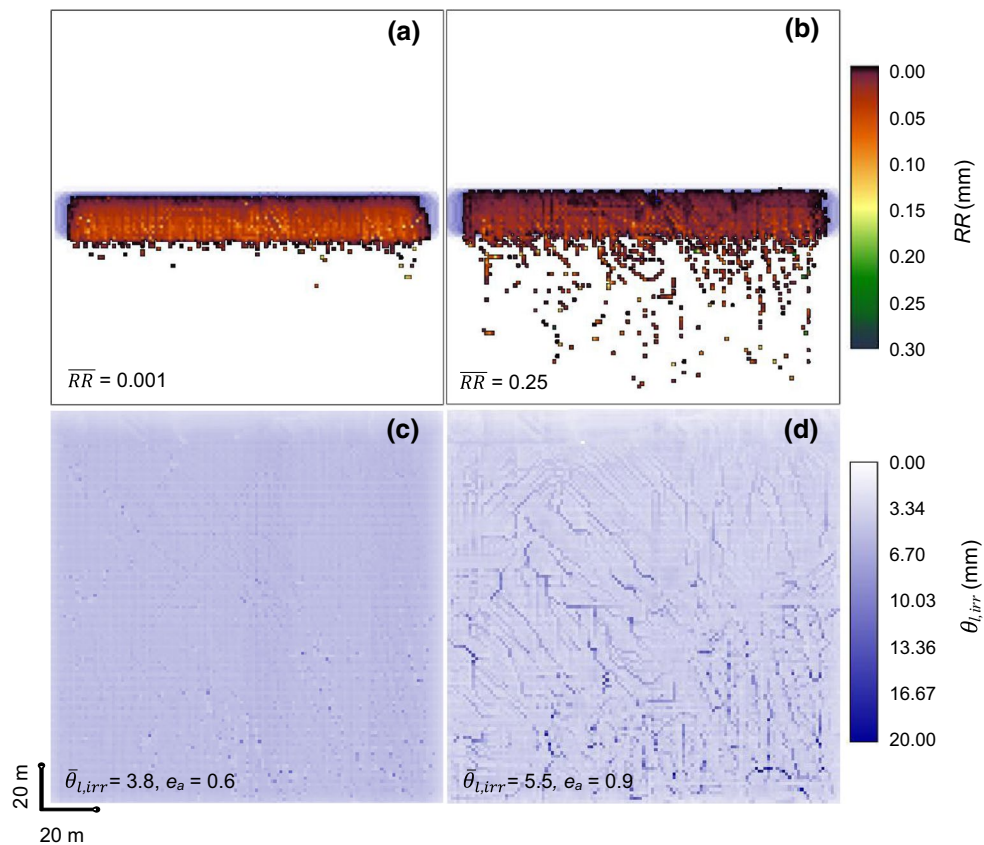

Fig. 4 **a–b** CREST model maps estimates of runoff–runon depth (RR, mm) at mid irrigation turn duration and soil moisture depth increase due to irrigation ($\bar{\theta}_{l,irr}$, mm) at the end of irrigation turn duration in scenarios (see Table 2): **a–c** $S1V3ND3\bar{\theta}_{l,a}1$, **b–d** $S2V3ND1\bar{\theta}_{l,a}3$

in wet areas on surface runoff generation, because each field situation is unique and must be considered independently. In this regard, Liu et al. (2011) measured the

infiltration capacity of a clay loam soil of a cultivated field in China using a rainfall simulator under three levels of $\bar{\theta}_{l,a}$. The authors observed that the infiltration capacity

Fig. 5 CREST model outputs: irrigation application efficiency (e_a), average soil moisture depth increase due to irrigation ($\bar{\theta}_{l,\mathrm{irr}}$), irrigation turn length efficiency (e_t) and runoff–runon factor (RRF) at all ($n = 81$) simulated scenarios. Scenario legends in *x-axis* as indicated in Table 2
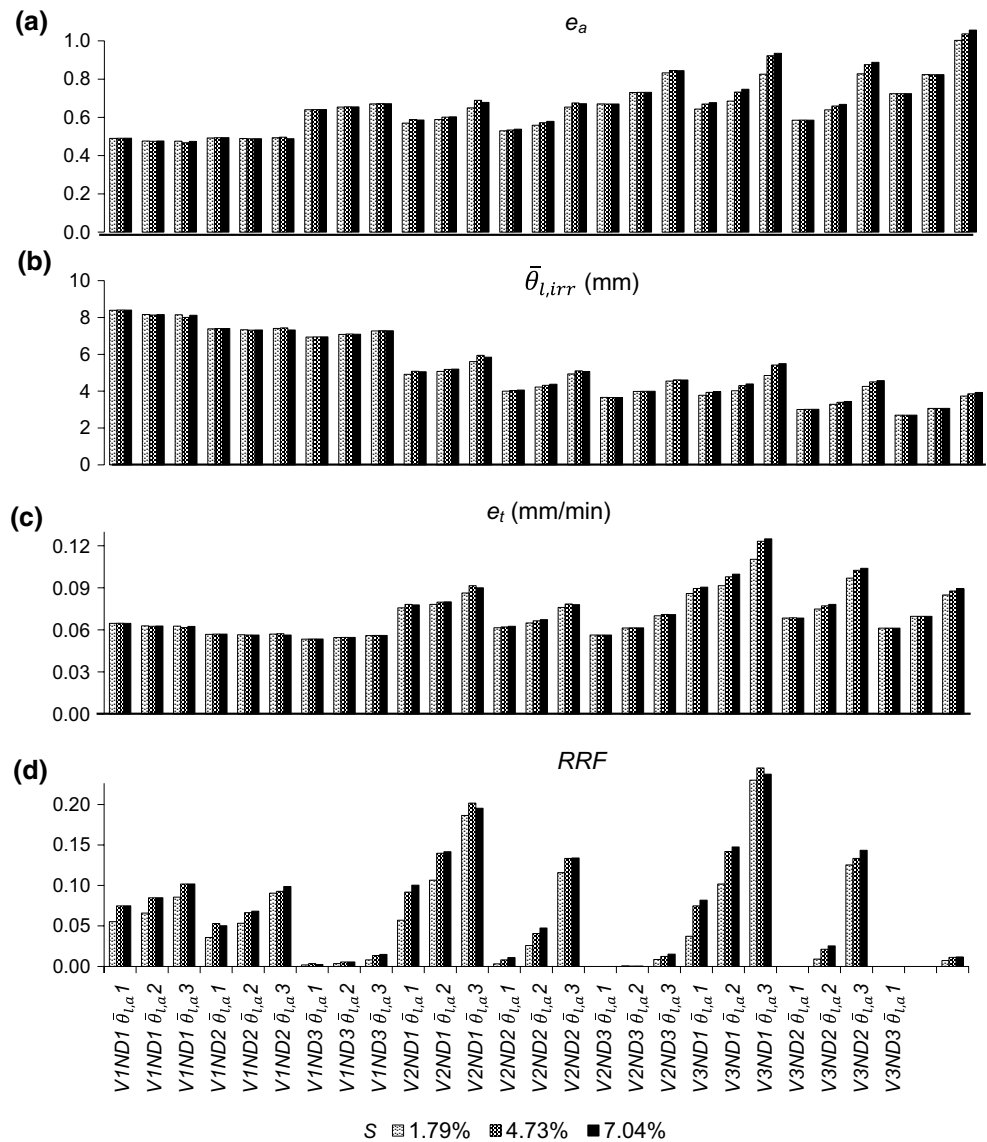
decreased with increasing initial water content of the soil, due to the low hydraulic gradient at the wetting front (Blackburn 1975).

Figure 5 shows main output results of CREST corresponding to all ($n = 81$) irrigation scenarios (see identifying acronyms along the x-axis) simulated in this study. The main ordering trend of the scenarios from left to right in the x-axis corresponds to increasing advance velocity (*V1, V2 and V3*). Each group of scenarios at a velocity level is secondary ordered by increasing sprinkler spacing along the linear-move span (*ND1, ND2 and ND3*) (which correspond to decreasing irrigation depth), and these latter groups are in turn subordinated along increasing antecedent soil moisture at irrigation start ($\bar{\theta}_{l,a}1, \bar{\theta}_{l,a}2, \bar{\theta}_{l,a}3$). The increasing gray levels in the bars correspond to increasing terrain slope.

The irrigation turn duration (ITD) decreases with increasing advance velocity (*V*) and consequently the

cumulative irrigation flow depth ($I_{r,a}$) or total amount of water spent during the irrigation turn. At high irrigation flows (*V1* and some *V2* groups, Fig. 5a, left side), the efficiency of irrigation application (e_a) does not vary with either ND or the terrain slope *S*. At low irrigation flows (some *V2* and *V3* groups, Fig. 5a, right side), e_a increases because of diminishing $I_{r,a}$ or increasing antecedent moisture $\bar{\theta}_{l,a}$ (see Eq. 5). Slope *S* has a minor effect on e_a.

The soil moisture depth attained through irrigation ($\bar{\theta}_{l,\mathrm{irr}}$, Fig. 5b) diminishes with increasing *V* as a consequence of a reduction in the cumulative irrigation flow $I_{r,a}$. At the low *V* range, the time efficiency (e_t, Eq. 6) is indifferent to $\bar{\theta}_{l,a}$ (Fig. 5c, left side) but increases with increasing antecedent moisture at high *V* scenarios (Fig. 5c, right side). This latter can be explained by considering the similar trends occurring in the runoff factor RRF (Fig. 5d). In scenarios of high antecedent moisture $\bar{\theta}_{l,a}$ corresponding to situations where the
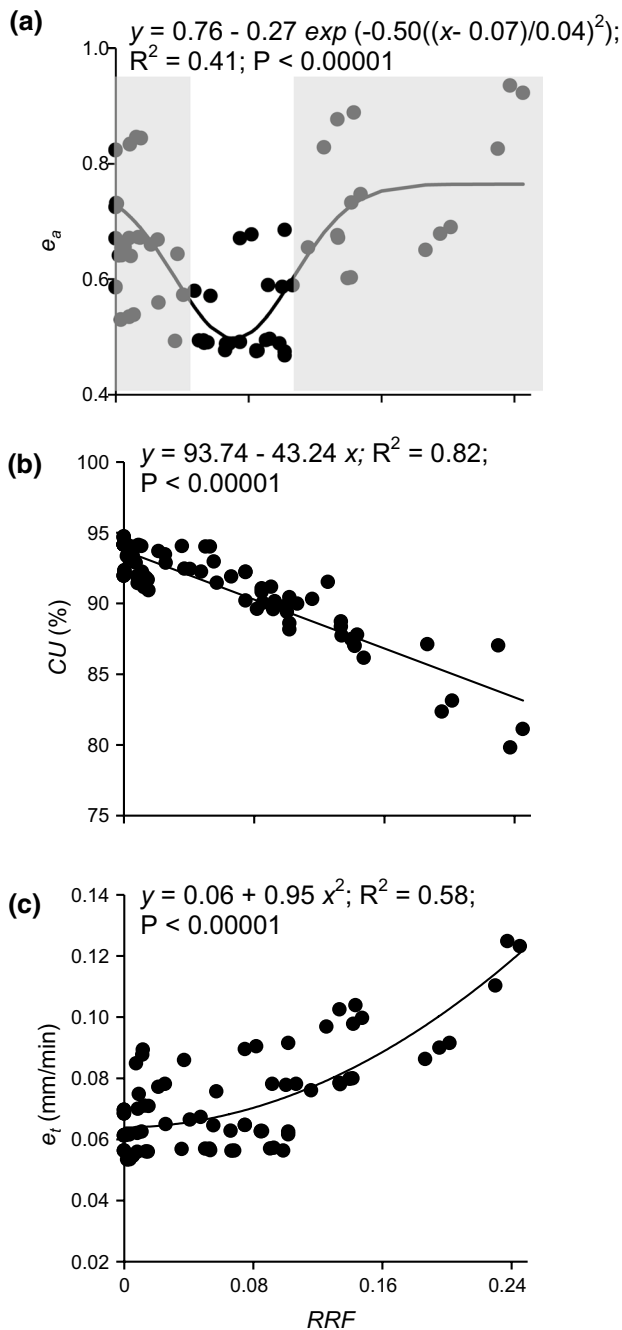
(a)

$y = 0.76 - 0.27\ exp\ (-0.50((x-\ 0.07)/0.04)^2);$
$R^2 = 0.41;\ P < 0.00001$

(b)

$y = 93.74 - 43.24\ x;\ R^2 = 0.82;$
$P < 0.00001$

(c)

$y = 0.06 + 0.95\ x^2;\ R^2 = 0.58;$
$P < 0.00001$

Fig. 6 Relations of **a** irrigation application efficiency (e_a) ~ runoff–runon factor (RRF), **b** coefficient of uniformity (*CU*) ~ RRF and **c** irrigation turn duration efficiency (e_t) ~ RRF

Table 4 Stepwise linear regression model of CREST input–output variables corresponding to scenarios at the high (*RRF* > 0.107) group

Predictor variables	Coefficients	t	P	R^2	df
S	0.141	2.272	0.039	0.947	13
V	0.824	13.327	0.000		
$\bar{\theta}_{l,a}$	0.425	6.840	0.000		

Model: $e_a = aS + bV + c\bar{\theta}_{l,a}$

It is of interest to inspect the role of runoff–runon in relation to irrigation efficiencies as defined in Eqs. (5–6) and CU (Eq. 8) through their binary interactions with RRF (Fig. 6).

The relation e_a ~ RRF (Fig. 6a) shows a trend (inverted normal) that can be significantly fitted to the e_a values. The gray areas in Fig. 6a, at RRF < 0.036 and RRF > 0.107, where these values correspond to the standard deviations of the normal function fitting e_a, identify the ranges of RRF where high application efficiencies occur.

CU ~ RRF (Fig. 6b) shows that the uniformity of soil moisture at the end of the irrigation turn steadily diminishes with increasing RRF. These results are consistent with studies indicating that the runoff–runon flow occurs as shallow sheets of water with threads of deeper, faster flow diverging and converging around surface protuberances interspersed with patterns of finely branched small channels following the heterogeneous soil surface in the *x–y* plane (Abrahams et al. 1990).

The relation e_t ~ RRF (Fig. 6c) was significantly fitted to an exponential equation where high values of e_t correspond to high values of RRF. In the irrigation practice, the turn duration implies related costs associated with it (labor, fuel, depreciation of equipment and maintenance costs) that usually are the subject of management for minimization.

Figure 6 summarizes the major compromise involved in adjusting the irrigation flow in order to maximize both e_a and e_t. According to Fig. 6a, c, this can only be achieved at RRF > 0.107, where CU would drop to 80–95 (Fig. 6b), which is still an acceptable uniformity for linear-move irrigation systems (Hanson 2005).

At scenarios with prevailing low runoff–runon conditions (*R*RF < 0.036), e_a and CU can be high, but at the expense of low e_t. These scenarios correspond to operations on nearly flat terrain, with a fast irrigation machine and relatively wide spaced sprinklers, resulting in low water application rates. Under these conditions, $I_{n,s} \cong Irr$ and $I_{n,p} \cong 0$. Operations with prevailing high runoff–runon (RRF > 0.107) can attain both high e_a and e_t, provided runoff–runon is controlled to an extent that would not produce undesirably low CU levels. These scenarios can be developed under relatively high irrigation flows, eventually on sloping terrain where $(I_{n,s} + I_{n,p}) = Irr$ and $I_{n,p} > 0$. In these

irrigation turn starts at relatively humid field conditions, runoff occurs relatively soon after irrigation start, and additional infiltration occurs under the runoff plumes, which increases $\bar{\theta}_{l,\mathrm{irr}}$ (Eq. 6). The runoff–runon factor (RRF) is relatively independent from *V* but shows wide variations depending on the antecedent soil moisture depth ($\bar{\theta}_{l,a}$). The field slope (*S*) modifies the RRF particularly at high *V* conditions.

latter cases; however, RR and e_a may depend on antecedent terrain characteristics or the boundary conditions (slope, moisture content) and management factors modifying the irrigation flow. Stepwise regression models (Table 4) separately performed on the high RRF group of Fig. 6 identified S, V and $\bar{\theta}_{l,a}$ as major controllers of e_a.

Conclusions

A modified CREST model was developed to simulate linear-move irrigation systems. The model was calibrated based on ad hoc micro-plot experiments to obtain estimates of infiltration and runoff–runon rates in semiarid areas representative of the Patagonian Monte.

Model simulations of irrigation scenarios supply hypotheses to be tested in applied irrigation studies. In a model, variables are handled consistently based on hydrological principles. A simulation model summarizes the interrelations among the many hydrological and management variables involved in irrigation and helps constructing analysis and observation of field situations.

The results obtained in this study indicate that under circumstances, both the application efficiency and the turn duration efficiency of linear-move sprinkler systems can be simultaneously maximized by considering terrain and management circumstances that would result in controlled (not null) runoff–runon flows on the irrigated terrain. Circumstances to be considered are the prevailing terrain slope and antecedent soil moisture, and the characteristics of the irrigation equipment controlling the irrigation flow (advance velocities and sprinkler spacing).

References

Abraham E, del Valle H, Roig F, Torres L, Ares J, Coronato F, Godagnone R (2009) Overview of the geography of the Monte desert of Argentina. J Arid Environ 73:144–153

Abrahams AD, Parsons AJ, Luk S (1990) Field experiments on the resistance to overland flow on desert hillslopes. Erosion, Transport and Deposition Processes. In: Proceedings of the Jerusalem workshop, Jerusalem, March–April 1990, IAHS Publ. no. 189

Antoine M (2010) Overland flow connectivity: theory and application at the interrill scale. Dissertation, Universite catholique de Louvain

Antoine M, Javaux M, Bielders C (2009) What indicators can capture runoff-relevant connectivity properties of the micro-topography at the plot scale? Adv Water Resour 32(8):1297–1310

Antoine M, Chalon C, Darboux F, Javaux M, Bielders C (2011a) Estimating changes in effective values of surface detention, depression storage and friction factor at the interrill scale, using a cheap and fast method to mold the soil surface microtopography. Catena 91:10–20

Antoine M, Javaux M, Bielders C (2011b) Integrating subgrid connectivity properties of the micro-topography in distributed runoff models, at the interrill scale. J Hydrol 403(3–4):213–223

Appels WM, Bogaart PW, van der Zee SE (2011) Influence of spatial variations of microtopography and infiltration on surface runoff and field scale hydrological connectivity. Adv Water Resour 34(2):303–313

Armindo RA, Botrel TA, Garzella TC (2011) Flow rate sprinkler development for site-specific irrigation. Irrig Sci 29:233–240

Bazzani GM (2005) An integrated decision support system for irrigation and water policy design: DSIRR. Environ Model Softw 20:153–163

Bisigato AJ, Bertiller MB (1999) Seedling emergence and survival in contrasting soil microsites in Patagonian Monte shrubland. J Veg Sci 10:335–342

Blackburn WH (1975) Factors influencing infiltration and sediment production of semiarid rangelands in Nevada. Water Resour Res 11(6):929–937

Castanon G (1992) The automation irrigation. Maquinas Tractors Agricolas 3(2):45–49

Causapé J, Quílez D, Aragüés R (2004) Assessment of irrigation and environmental quality at the hydrological basin level. I. Irrigation quality. Agric Water Manag 70:195–209

Ceballos A, Martínez-Fernández J, Santos F, Alonso P (2002) Soil-water behaviour of sandy soils under semi-arid conditions in the Duero Basin (Spain). J Arid Environ 51:501–519

Christiansen JE (1941) The uniformity of application of water by sprinkler systems. Agric Eng 22:89–92

Chu X, Yang J, Chi Y, Zhang J (2013) Dynamic puddle delineation and modeling of puddle to-puddle filling-spilling-merging-splitting overland flow processes. Water Resour Res. doi:10.1002/wrcr.20286

Connell LD, Gilfedder M, Jayatilaka C, Bailey M, Vandervaere JP (1999) Optimal management of water movement in irrigation bays. Environ Modell Softw 14:171–179

Darboux F, Davy Ph, Gascuel-Odoux C, Huang C (2001) Evolution of soil surface roughness and flowpath connectivity in overland flow experiments. Catena 46:125–139

Darboux F, Gascuel-Odoux C, Davy P (2002) Effects of surface water storage by soil roughness on overland-flow generation. Earth Surf Process Landf 17(3):223–233

DeBoer DW, Monnens MJ, Kincaid DC (2000) Rotating-plate sprinkler spacing on continuous-move irrigation laterals. National irrigation symposium. In: Proceedings of the 4th decennial symposium. ASAE. November 14–16, Phoenix, Arizona, pp 115–122

del Valle HF (1998) Patagonian soils: a regional synthesis. Ecol Austral 8:103–123

Elliot RL, Nelson JD, Lofits JC, Hart WE (1980) Comparison of sprinkler uniformity models. ASCE J Irrig Drain Eng 106:321–330

Ewen J (2011) Hydrograph matching method for measuring model performance. J Hydrol 408:178–187

Fernández-Cirelli A, Arumí JL, Rivera D, Boochs PW (2009) Environmental effects of irrigation in arid and semi-arid regions. Chilean J Agric Res 69:27–40

Foley JL, Silburn DM (2002) Hydraulic properties of rain impact surface seals on three clay soils—influence of raindrop impact frequency and rainfall intensity during steady state. Aust J Soil Res 40:1069–1083

Gee GW, Bauder JW (1986) Particle-size analysis. In: Klute A (ed) Methods of soil analysis, part 1, physical and mineralogical methods, 2nd edn. Agronomy Monograph No. 9, ASA-SSSA

Gencoglan C, Gencoglan S, Merdun H, Ucan K (2005) Determination of ponding time and number of on–off cycles for sprinkler irrigation applications. Agric Water Manag 72:47–58

Hanson B (2005) Irrigation system design and management: implications for efficient nutrient use. Western Nutrient Management Conference, Salt Lake City, UT, 6:38–45

Hart WE (1961) Overhead irrigation pattern parameters. Agric Eng 42(7):354–355

Hillel D (1998) Environmental soil physics. Academic Press, New York

ISO 11272 (1998) Deutsches Institut für Normung—soil quality—determination of dry bulk density. Beuth Verlag, Berlin

James LG (1988) Principle of farm irrigation system design. Wiley, New York, pp 543

James LG, Larson CL (1976) Modeling infiltration and redistribution of soil water during intermittent application. Trans ASAE 19:482–488

Jensen S, Domingue J (1988) Extracting topographic structure from digital elevation data for geographic information system analysis. Photogramm Eng Remote Sens 54(11):1593–1600

Jorge J, Pereira LS (2003) Simulation and evaluation of set sprinkler systems with AVASPER. In: Improved irrigation technologies and methods (Proceedings of ICID international workshop, Sep. 2003), Association Française des Irrigations et du Drainage, AFEID, Montpellier, CD-ROM Paper 21

Keller J, Bliesner RD (2000) Sprinkler and trickle irrigation. The Blackburn Press, Caldwell

Legout C, Darboux F, Nédélec Y, Hauet A, Esteves M, Renaux B, Denis H, Cordier S (2012) High spatial resolution mapping of surface velocities and depths for shallow overland flow. Earth Surf Process Landf 37:984–993

Leonard J, Esteves M, Perrier E, de Marsily G (1999) A spatialized overland flow approach for the modelling of large macropores influence on water infiltration. International Workshop of EurAgEng's Field of Interest on Soil and Water, Leuven, pp 313–322

Li J, Kawano H (1996) The areal distribution of soil moisture under sprinkler irrigation. Agric Water Manag 32:29–36

Li X, Contreras S, Solé-Benet A, Cantón Y, Domingo F, Lázaro R, Lin H, Van Wesemael B, Puigdefábregas J (2011) Controls of infiltration–runoff processes in Mediterranean karst rangelands in SE Spain. Catena 86:98–109

Liu H, Lei TW, Zhao J, Yuan CP, Fan YT, Qu LQ (2011) Effects of rainfall intensity and antecedent soil water content on soil infiltrability under rainfall conditions using the run off-on-out method. J Hydrol 396:24–32

Mao LL, Lei TW, Li X, Liu H, Huang XF, Zhang YN (2008) A linear source method for soil infiltrability measurement and model representations. J Hydrol 353:49–58

Mares MA, Morello J, Goldstein G (1985) Semi-arid shrublands of the world. In: Evenari M, Noy-Meir I, Goodall D (eds) Hot deserts and arid shrublands, ecosystems of the world. Elsevier, Amsterdam, pp 203–237

McLean RK, Sri Ranjan R, Klassen G (2000) Spray evaporation losses from sprinkler irrigation systems. Can Agric Eng 42(1):1–15

Mein RG, Larson CL (1973) Modeling infiltration during a steady rain. Water Resour Res 9(2):384–394

Merot A, Bergez JE (2010) IRRIGATE: a dynamic integrated model combining a knowledge-based model and mechanistic biophysical models for border irrigation management. Environ Model Softw 25:421–432

Molle B, Legat Y (2000) Model for water application under pivot sprinkler. II: calibration and results. ASCE. J Irrig Drain Eng 116(6):348–354

Montero J, Tarjuelo JM, Carrión P (2001) SIRIAS: a simulation model for sprinkler irrigation II. Calibration and validation of the model. Irrig Sci 20:85–98

Morello JH (1984) Perfil Ecológico de Sud America. Instituto de Cooperación Iberoamericana, Madrid

Morvant JK, Dole JM, Ellen E (1997) Irrigation systems alters distribution of roots, soluble salts, nitrogen and pH in the root medium. Hort Technol 7:156–160

Mügler C, Planchon O, Patin J, Weill S, Silvera N, Richard P, Mouche E (2011) Comparison of roughness models to simulate overland flow and tracer transport experiments under simulated rainfall at plot scale. J Hydrol 402:25–40

Mulas P (1986) Developments in the automation of irrigation. Colture Protelte 15(6):17–19

Ohrstrom P, Persson M, Albergel J, Zante P, Nasri S, Berndtsson R, Olsson J (2002) Field-scale variation of preferential flow as indicated from dye coverage. J Hydrol 257:164–173

Olaya V (2004) A gentle introduction to SAGA GIS. The SAGA User Groupe, Gottingen

Olaya V, Conrad O (2009) Geomorphometry in SAGA. In: Hengl T, Reuter HI (ed) Geomorphometry concepts, software, applications. Developments on soil science, vol 33. Elsevier, UK, pp 765

Parsons AJ, Wainwright J (2006) Depth distribution of inter-rill overland flow and the formation of rills. Hydrol Process 20:1511–1523

Pedras CM, Pereira LS (2006) A DSS for design and performance analysis of microirrigation systems. In: Zazueta F, Xin J, Ninomiya S, Schiefer G (ed) Computers in agriculture and natural resources (Proceedings of 4th World Congress, Orlando FL). ASABE, St Joseph, MI, pp 666–671

Reaney SM (2008) The use of agent based modelling techniques in hydrology: determining the spatial and temporal origin of channel flow in semi-arid catchments. Earth Surf Process Landf 33:317–327

Richards JA (1986) Remote sensing digital image analysis: an introduction. Springer, Berlin

Rodríguez JA, Martos JC (2010) SIPAR_ID: freeware for surface irrigation parameter identification. Environ Model Softw 25:1487–1488

Rossi MJ, Ares JO (2012a) Close range stereo-photogrammetry and video imagery analyses in soil eco-hydrology modelling. Photogramm Rec 27(137):111–126

Rossi MJ, Ares JO (2012b) Depression storage and infiltration effects on overland flow depth-velocity-friction at desert conditions: field plot results and model. Hydrol Earth Syst Sci 16:3293–3307

Rostagno CM, del Valle HF, Videla L (1991) The influence of shrubs on some chemical and physical properties of an aridic soil in north-eastern Patagonia, Argentina. J Arid Environ 20:179–188

Schaap MG, Leij FJ (1998) Database related accuracy and uncertainty of pedotransfer functions. Soil Sci 163:765–779

Silva LL (2007) Fitting infiltration equations to centre-pivot irrigation data in a Mediterranean soil. Agric Water Manag 94:83–92

Smith MW, Cox NJ, Bracken LJ (2011) Modeling depth distribution of overland flows. Geomorphol 125:402–413

Soil Survey Staff (1999) Soil taxonomy: a basic system of soil classification for making and interpreting soil surveys. Agricultural Handbook 436, USDA Soil Conservation Service. US Government Printing Office, Washington, DC

Tarjuelo JM, Valiente M, Lozoya J (1992) Working condition of sprinkler to optimize application of water. ASCE J Irrig Drain Eng 118(6):895–913

Tatard L, Planchon O, Wainwright G, Nord J, Favis-Mortlock D, Silvera N, Ribolzi O, Esteves M, Huang CH (2008) Measurement and modelling of high-resolution flow-velocity data under simulated rainfall on a low-slope sandy soil. J Hydrol 348:1–12

Uva WL, Weiler TC, Milligan RA (1998) A survey on the planning and adoption of zero run-off subirrigation systems in greenhouse operations. Hort Sci 34:660–663

van Schaik NL (2009) Spatial variability of infiltration patterns related to site characteristics in a semi-arid watershed. Catena 78:36–47

Wang J, Yang H, Gourley J, Sadiq IK, Yilmaz K, Adler R, Policelli F, Habib S, Irwn D, Limaye A, Korme T, Okello L (2011) The coupled routing and excess storage (CREST) distributed hydrological model. Hydrol Sci J 56(1):84–98

Warrick AW (1983) Interrelationship of irrigation uniformity parameters. ASCE J Irrig Drain Eng 109:317–332

Warrick AW, Gardner WR (1983) Crop yield as affected by spatial variations of soil and irrigation. Water Resour Res 19:181–186

Weiler M, Naef F (2003) Simulating surface and subsurface initiation of macropore flow. J Hydrol 273:139–154

Wilmes GJ, Martin DL, Supalla RJ (1993) Decision support system for design of center pivots. Trans ASAE 37(1):165–175

Wooding RA (1968) Steady infiltration from a shallow circular pond. Water Resour Res 4:1259–1273

Ye KQ (1998) Orthogonal column Latin hypercubes and their application in computer experiments. J Am Stat Assoc 93(444):1430–1439

Zhang L, Merkley GP, Pinthong K (2013) Assessing whole-field sprinkler irrigation application uniformity. Irrig Sci 31:87–105